Esaki spin diode based on composite graphene superlattices

J. Munárriz,[1] C. Gaul,[1,2] A. V. Malyshev,[1,3] P. A. Orellana,[4] C. A. Müller,[5] and F. Domínguez-Adame[1]

[1] *GISC, Departamento de Física de Materiales, Universidad Complutense, E-28040 Madrid, Spain*
[2] *CEI Campus Moncloa, UCM-UPM, Madrid, Spain*
[3] *Ioffe Physical-Technical Institute, 26 Politechnicheskaya str., 194021 St-Petersburg, Russia*
[4] *Departamento de Física, Universidad Católica del Norte, Casilla 1280, Antofagasta, Chile*
[5] *Centre for Quantum Technologies, National University of Singapore, Singapore 117543, Singapore*

(Dated: November 1, 2012)

PACS numbers: 72.80.Vp, 72.20.Ht, 85.75.Mm

Since the pioneering work by Esaki[1], quantum tunneling and negative differential resistance (NDR) have been the underlying principle of operation of various quantum devices[2–4]. The principle implies that the electric current through a device increases when the chemical potential in one of the leads approaches an energy level of the device. However, if the energy level depends on the applied voltage the current can decrease drastically with a further increase of the voltage, resulting in the NDR.

Such conductance anomaly can be observed in semiconductor heterostructures[2], molecular systems[4] and at the atomic scale[5]. Here we address a novel device based on graphene, whose remarkable charge transport properties[6] and long spin-coherence length[7] makes it a promising material for spintronics[8,9]. We consider a composite superlattice comprising a set of ferromagnetic insulator strips deposited on top of a graphene nanoribbon (GNR). We calculate current–voltage characteristics of the device and predict spin-filtering effect and strong spin-dependent NDR.

The proposed system is composed of a rectangular GNR of width $W \simeq 9.8\,\mathrm{nm}$, connected to source and drain leads, and $N = 5$ rectangular strips of a ferromagnetic insulator arranged periodically on top of the GNR (see the upper panel of Fig. 1). The width of the strips is $a = 23.9\,\mathrm{nm}$ and the spacing between them is $b = 55.8\,\mathrm{nm}$. It is known that both the width and the edge type of a GNR strongly affect its electronic properties. Both the experimental evidence[10] and *ab-initio* calculations[11] show that the spectrum of a GNR with armchair edges has a band gap, which is inversely proportional to the width W and depends on the remainder $(W/a_0 \mod 3)$ (where $a_0 = 0.246\,\mathrm{nm}$ is the width of the graphene lattice hexagon). Contrary to GNRs with zigzag edges, the dispersion relation of the armchair GNR is centered around $k = 0$; the latter is advantageous for tunneling structures, such as a superlattice, because resonant levels are expected to be broader and less affected by disorder[12]. We therefore restrict ourselves to the armchair GNRs.

EuO can be used as the ferromagnetic insulator; this material has been studied in conjunction with graphene both experimentally[13] and theoretically[14]. The exchange interaction between magnetic ions in the strips and charge carriers in the GNR can be described as an effective Zeeman splitting $\pm\Delta_{\mathrm{ex}}$ of the spin sublevels[14]. There is still no consensus on the magnitude of the exchange splitting amplitude Δ_{ex} in graphene. We use $\Delta_{\mathrm{ex}} = 5\,\mathrm{meV}$, which lies in the range of values known from the literature $(3 - 10\,\mathrm{meV})$[14–16]. We have checked that our results do not change qualitatively if we use a different value of Δ_{ex} from the known range.

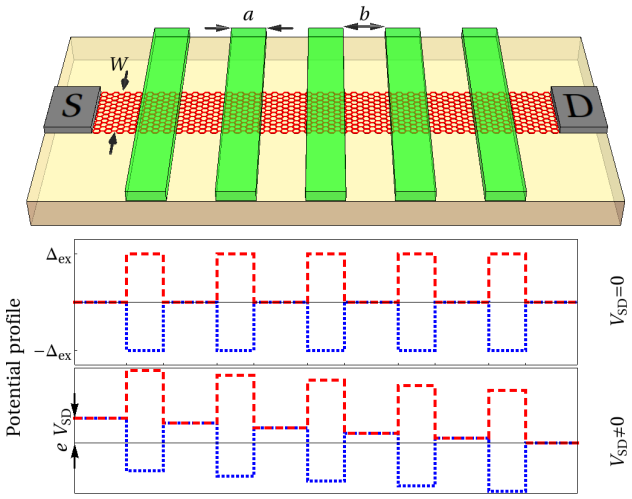

FIG. 1. **Device design and potential profiles.** Upper panel shows the schematics of the device: a GNR, connected to source (S) and drain (D) leads, with 5 perpendicular strips of a ferromagnetic insulator (green bars) placed on top of it. Potential profiles for spin-up (dotted red lines) and spin-down (dashed blue lines) electrons in the unbiased and biased devices are shown in the middle and lower panels respectively.

Because the exchange interaction has the characteristic length scale of one atomic layer, the splitting is induced only in the regions of the GNR which are just below the ferromagnetic strips. Therefore, for the chosen system geometry, a spin-up (spin-down) electron propagating along the sample will be subjected to a potential comprising a periodic set of rectangular barriers (wells), as plotted in the middle panel of Fig. 1. In other words, the array of the ferromagnetic strips creates a spin-dependent

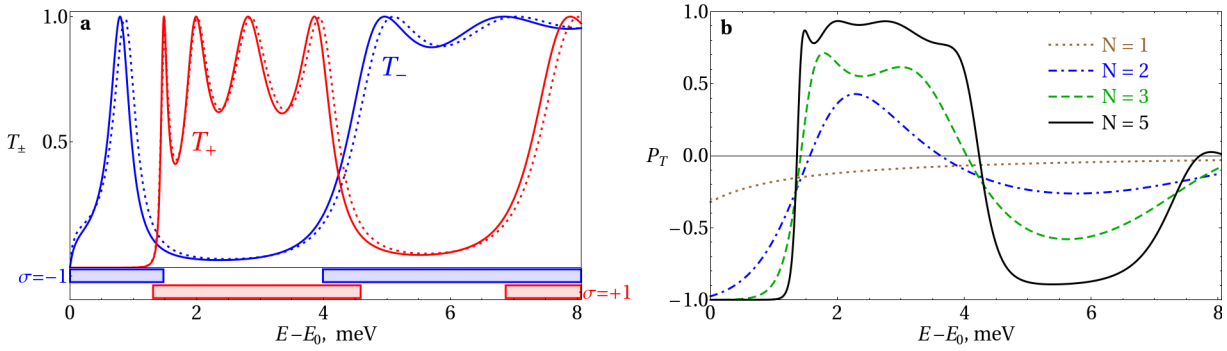

FIG. 2. **Transmission and its polarization for the unbiased device.** **a**, transmission coefficients $T_\pm$ as functions of energy for spin-up (red) and spin-down (blue) electrons. There is a very good agreement between the Dirac transfer-matrix theory (solid lines) and the tight-binding calculation (dotted lines). The origin of the energy for each curve is set to the lowest subband edge E_0 calculated within the corresponding model. Horizontal bars in the lower part of the figure indicate transmission bands of the infinite superlattice. **b**, transmission polarization P_T as a function of energy for different numbers N of ferromagnetic strips.

superlattice. We note that similar systems manifesting the NDR have been studied[17], however the superlattice potential was supposed to be induced by electrostatic gates, so all characteristics were spin independent.

Calculation methods and techniques. For not too narrow GNRs the low energy excitations can be treated very efficiently within the Dirac approximation[18,19]. The boundary conditions at the GNR edge can be met by a superposition of two states from different valleys. The transverse momentum $k_{\perp n}$ (measured from the respective Dirac point) is quantized[20], and the longitudinal momentum $k_\parallel$ obeys the dispersion relation $E_n(k_\parallel) = \pm\hbar v_{\rm F}(k_{\perp n}^2 + k_\parallel^2)^{1/2}$. In our case $W = 40\,a_0$ and the minimum transverse momentum is $k_\perp = \pi/[3(W + a_0)]$[21]. The resulting gap is an important feature of the model because it eliminates the Klein tunneling effect which would always result in full transmission and current leakage.

For the chosen geometry, the potential depends only on the longitudinal coordinate x, and the transverse momentum $k_\perp$ is conserved. Therefore it suffices to solve for the longitudinal wave function $\phi_\parallel(x)$. The solution of the Dirac equation within each interval of constant potential value V_j is the superposition of two counter-propagating sublattice pseudo-spinors. Both the longitudinal momentum k_j and the spinor components depend on the energy E of the injected carrier and the local potential V_j. At each junction the wave vector k_j changes while the wave function remains continuous. The free propagation across the intervals and the continuity at the interfaces can be cast in a transfer-matrix formalism, which ultimately yields the transmission and reflection of the (finite) system, as function of energy[21].

Transmission at zero bias. Because the superlattice potential depends on the carrier spin, the transmission coefficient $T_\pm$ is also spin-dependent. Hereafter, + (−) signs and red (blue) colors in all figures correspond to spin-up (spin-down) electrons respectively. Figure 2 **a** shows the transmission probability through the unbiased sample calculated within the Dirac approximation (solid lines) and the full tight-binding model (dotted lines), which is more accurate[21]. The figure demonstrates very good agreement between the two approaches. The Dirac model overestimates slightly the lowest subband edge position E_0 (by 0.3%), due to the $\boldsymbol{k}\cdot\boldsymbol{p}$ approximation in the derivation of the Dirac equation, which breaks down for very narrow GNRs[20]. In the following, we use exclusively the Dirac transfer-matrix method since it requires less computational resources. Furthermore, the formalism can be applied to study the system as the number of strips $N \to \infty$, and gain physical insight into the main features of the transmission[21,22]. For an unbiased infinite superlattice, an eigenfunction has the Bloch phase factor $\exp(\pm iKl)$ which is the eigenvalue of the transfer matrix $\widetilde{G}$ across one superlattice cell of the length $l = a + b$. Thus, the dispersion relation for a GNR is implicitly defined by the equation $\cos(Kl) = \mathrm{Tr}(\widetilde{G})/2$. If $|\,\mathrm{Tr}(\widetilde{G})| > 2$, there is no propagating solution and the corresponding energy E falls into the bandgap of the superlattice.

The transmission spectrum, shown in Fig. 2 **a**, is typical for a superlattice. Already for $N = 5$, the regions of high transmission coincide quite well with the bands of the infinite superlattice given by the horizontal bars at the bottom of the figure. The spectrum is spin-dependent, which manifests itself clearly in the transmission polarization, defined as $P_T = (T_+ - T_-)/(T_+ + T_-)$, shown in Fig. 2 **b**.

As the number of strips is increased, the transmission of modes with energies outside the transmission bands vanishes rapidly, thus leading to an enhanced polarization. For $N \geq 3$, the transmission polarization manifests rapid changes in almost the whole range of its possible values $(-1, 1)$ within narrow energy intervals. Such abrupt polarization switching can be expected only if the overlap between transmission bands corresponding to different spins is small (see Fig. 2 **a**). The band overlap is

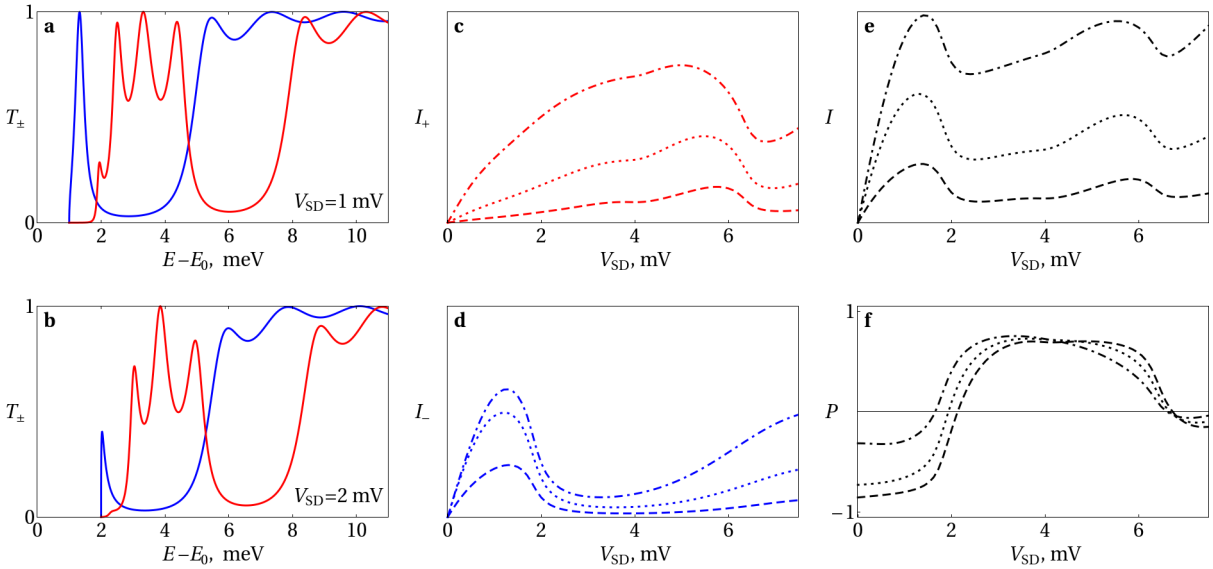

FIG. 3. **Transmission and currents at finite bias.** Panels **a** and **b** show that the transmission bands for both spins at finite bias V_{SD} are shifted, quenched and distorted compared to the unbiased case (Fig. 2 **a**). Panels **c** and **d** display the spin-polarized currents $I_\pm$ as functions of the bias V_{SD}, for $T = 4\,\mathrm{K}$ and different values of the chemical potential: $\mu - E_0 = 0\,\mathrm{meV}$ (dashed), $0.5\,\mathrm{meV}$ (dotted), and $1.0\,\mathrm{meV}$ (dash-dotted) lines. Finally, panels **e** and **f** show the total current I and the current polarization P for the same parameters.

determined by the relationship between different parameters: the splitting amplitude Δ_{ex} and the superlattice geometrical parameters a and b, which should be chosen carefully in order to observe a pronounced switching and filtering effect in a real world device[21]. Such a choice can be made, for example, by analyzing the transmission spectrum of the infinite lattice in the Dirac model.

Spin-polarized current at finite bias. We finally use the obtained transmission coefficients $T_\pm$ to calculate the spin-polarized electric current within the Landauer-Büttiker scattering formalism[21,23]. We address the current and its polarization at a finite bias V_{SD} between source and drain, whose chemical potentials, $\mu_S = \mu + eV_{SD}$ and $\mu_D = \mu$, have the same offset μ from the band-gap center (the Dirac point). For simplicity, we assume that the source-drain voltage drops at the edges of the wells and barriers of the superlattices only, resulting in a piecewise potential profile as shown in the lower panel of Fig. 1. We have checked numerically that our results do not depend crucially on the details of the potential profile. The bias results in a distortion of the transmission bands: the bands shift to lower energies, become quenched and finally disappear as the voltage increases, as shown in Fig. 3 **a** and **b**.

The polarized currents $I_\pm$ as functions of V_{SD} are plotted in Fig. 3 **c** and **d**. The spin-dependent transmission bands and their distortion due to the bias lead to NDR regions at different values of the bias voltage for different spins. For the spin down, the NDR occurs at a lower bias and the negative slope of the $I - V$ curve is particularly steep. This is due to the fact that the first transmission peak remains very sharp while it is being quenched (see panels **a** and **b** of Fig. 3). The lowest spin-up transmission band disappears at a higher bias, when its profile is more washed out, resulting in the less pronounced NDR.

It is worthwhile to address the total current $I = I_+ + I_-$ through the device, as well as its polarization $P = (I_+ - I_-)/(I_+ + I_-)$. These quantities are plotted in the panels **e** and **f** of Fig. 3. Panel **e** shows that the total current I also manifests the NDR for two different biases, corresponding to the NDR regions of I_- and I_+. The current polarization shows an initial range with negative values followed by a second region dominated by the spin-up current. As the bias increases further the polarization decays and finally vanishes. Note that the current is highly polarized for certain biases, which proves that the device can operate as a spin filter. On the other hand, because the characteristics $I_\pm(V_{SD})$ are essentially different, if the source feeds partially polarized electrons, the total current through the device would depend on the degree of their polarization. The latter opens a possibility to determine the polarization of a current by purely electrical measurements, which is a very promising application.

We have considered an ideal device with perfect rectangular GNR and strips, while different imperfections and perturbations can introduce disorder into the system and affect the electric current and its polarization[24]. There are different possible sources of disorder, for example, charged impurities in the substrate or defects of the device fabrication. The former results in an additional smooth electrostatic potential and can hardly deteriorate the transmission through the device to a large extent. However, the effect of the latter on the transport proper-

ties can be stronger. To estimate the possible impact of the fabrication imperfections on the predicted effects, we considered disordered superlattices varying randomly the strip widths and spacings by up to 20%. Our calculations demonstrate that the transmission bands are affected by the disorder to a comparable degree for both spin up and spin down electrons, which suggests that a moderate disorder would not seriously deteriorate transport and polarization properties of the device. The current magnitude remains almost the same, and the NDR turns out to be robust under the effects of disorder as well.

In summary, we propose a novel graphene-based device comprising a GNR and a regular array of ferromagnetic strips on top of it. The ferromagnets induce an exchange splitting of electronic states in the GNR and create a spin-dependent superlattice. We have shown that the electric current through the device can be highly polarized. Thus, the device can operate as a spin filter. Alternatively, it can be used to obtain the polarization degree of the source electrons (the polarization of the "incoming" current) by purely electrical measurements. Moreover, the two polarized components of the current manifest non-monotonic dependencies on the source-drain voltage. In particular, for both spins, the current-voltage characteristics presents regions with negative differential resistance for the bias in the range of a few millivolts. The device operates therefore as a low-voltage Esaki diode for spin-polarized currents.

A prominent advantage of the usage of a superlattice induced by ferromagnets is that the exchange interaction is very short-ranged; its characteristic length scale is on the order of one monolayer. Unlike the long-range electrostatic gate potentials which can interfere with each other, setting a practical lower limit for the inter-device spacing, the exchange interaction induced potential profiles are very abrupt. Therefore, heterostructures created by ferromagnets allow for very close packing of circuits and, consequently, considerably higher device densities.

Finally, we note that in a spintronic device the degree of freedom that carries information is the polarization of the current rather than its magnitude. We have shown that the current polarization is also a non-monotonic function of the source-drain voltage in our proposed device, which suggests that it can be used as an Esaki spin diode. This opens a possibility to design a whole new class of true spintronic circuits such as spin oscillators, amplifiers and triggers.

[1] L. Esaki, Physical Review **109**, 603 (1958).
[2] L. Esaki, Reviews of Modern Physics **46**, 237 (1974).
[3] S. Sze and K. Ng, *Physics of Semiconductor Devices*, Wiley-Interscience publication, John Wiley & Sons (2006).
[4] A. V. Malyshev, Physical Review Letters **98**, 096801 (2007).
[5] P. Bedrossian, D. M. Chen, K. Mortensen, and J. A. Golovchenko, Nature **342**, 258 (1989).
[6] K. S. Novoselov, A. K. Geim, S. V. Morozov, D. Jiang, Y. Zhang, S. V. Dubonos, I. V. Grigorieva, and A. A. Firsov, Science **306**, 666 (2004).
[7] C. L. Kane and E. J. Mele, Physical Review Letters **95**, 226801 (2005).
[8] A. V. Rozhkov, G. Giavaras, Y. P. Bliokh, V. Freilikher, and F. Nori, Physics Reports **503**, 77 (2011).
[9] J. Munárriz, F. Domínguez-Adame, P. A. Orellana, and A. V. Malyshev, Nanotechnology **23**, 205202 (2012).
[10] M. Y. Han, B. Özyilmaz, Y. Zhang, and P. Kim, Physical Review Letters **98**, 206805 (2007).
[11] Y.-W. Son, M. L. Cohen, and S. G. Louie, Physical Review Letters **97**, 216803 (2006).
[12] J. Munárriz, F. Domínguez-Adame, and A. V. Malyshev, Nanotechnology **22**, 365201 (2011).
[13] D. F. Förster, *EuO and Eu on metal crystals and graphene: interface effects and epitaxial films*, PhD thesis, Universität zu Köln (2011).
[14] H. Haugen, D. Huertas-Hernando, and A. Brataas, Physical Review B **77**, 115406 (2008).
[15] J. Zou, G. Jin, and Y.-Q. Ma, Journal of Physics: Condensed Matter **21**, 126001 (2009).
[16] Y. Gu, Y. H. Yang, J. Wang, and K. S. Chan, Journal of Applied Physics **105**, 103711 (2009).
[17] G. J. Ferreira, M. N. Leuenberger, D. Loss, and J. C. Egues, Physical Review B **84**, 125453 (2011).
[18] P. R. Wallace, Physical Review **71**, 622 (1947).
[19] A. H. Castro Neto, F. Guinea, N. M. R. Peres, K. S. Novoselov, and A. K. Geim, Reviews of Modern Physics **81**, 109 (2009).
[20] L. Brey and H. A. Fertig, Physical Review B **73**, 235411 (2006).
[21] See the supplementary material of this Letter.
[22] M. Barbier, P. Vasilopoulos, and F. M. Peeters, Physical Review B **81**, 075438 (2010).
[23] M. Büttiker, Y. Imry, R. Landauer, and S. Pinhas, Physical Review B **31**, 6207 (1985).
[24] Q. Zhao, J. Gong, and C. A. Müller, Physical Review B **85**, 104201 (2012).
[25] J. Schelter, D. Bohr, and B. Trauzettel, Physical Review B **81**, 195441 (2010).
[26] C. S. Lent and D. J. Kirkner, Journal of Applied Physics **67**, 6353 (1990).
[27] D. Z. Y. Ting, E. T. Yu, and T. C. McGill, Physical Review B **45**, 3583 (1992).
[28] K. Wakabayashi, Y. Takane, M. Yamamoto, and M. Sigrist, New Journal of Physics **11**, 095016 (2009).

ACKNOWLEDGMENTS

Work in Madrid was supported by the MICINN (project MAT2010-17180). Research of C.G. was supported by the PICATA postdoctoral fellowship from the Moncloa Campus of International Excellence (UCM-UPM). P.A.O acknowledges financial support from the FONDECYT, under grant 1100560. CQT is a Research

Centre of Excellence funded by the Ministry of Education
and the National Research Foundation of Singapore.

SUPPLEMENT A. MODEL HAMILTONIAN

A simple tight-binding (TB) Hamiltonian of a single electron is widely used to model GNRs. For low energy excitations, *i.e.*, energies close to the Dirac point, the interaction can be restricted to nearest neighbors. Then, the Hamiltonian can be written as

$$\mathcal{H} = -t \sum_{\langle i,j \rangle} |i\rangle\langle j| + \sum_i \epsilon_{\rm SD}(x_i)|i\rangle\langle i| + \sigma\, \Delta_{\rm ex} \sum_{i\in\mathcal{L}} |i\rangle\langle i| \ . \tag{S1}$$

Here $|i\rangle$ is the ket vector of the atomic orbital of the ith carbon atom, $t = 2.8\,\text{eV}$ is the hopping between neighboring atoms, the full set of which is denoted as $\langle i, j\rangle$. The on-site energy is the superposition of the following two terms: the bias induced electrostatic potential $\epsilon_{\rm SD}(x_i)$, where x_i is the coordinate of the ith atom along the direction of the GNR, and the spin-dependent exchange-interaction shift $\Delta_{\rm ex}$ due to the ferromagnetic strips, with $\sigma = \pm 1$ for spin-up and spin-down electrons. The exchange-interaction is induced only at atoms that are in direct contact with the ferromagnetic strips (the full set of them is labeled as $\mathcal{L}$ in the above equation). Both terms are sketched in the middle and lower panels of Fig. 1 of the main text.

First, we calculate the wave function in the whole sample and the transmission coefficient. This is accomplished by assuming semi-infinite leads, whose modes are calculated using an effective transfer-matrix approach[25]. Then, both the ingoing and outgoing wave functions are computed as linear combinations of propagating plane waves at a given energy. The wave function in the GNR can be obtained using the quantum transmission boundary method[26,27]. This allows us to calculate the spin-dependent transmission coefficients $T_\pm$. Finally, we use the Landauer-Büttiker scattering formalism to calculate the spin-polarized electric current $I_\pm$ across the sample[23] as follows

$$I_\pm = \frac{2e}{h} \int T_\pm(E, V_{\rm SD}) \Big[f(E - \mu_{\rm S}) - f(E - \mu_{\rm D}) \Big] {\rm d}E \ , \tag{S2}$$

where $f(\epsilon) = [\exp(\epsilon/k_{\rm B}T) + 1]^{-1}$ is the Fermi-Dirac distribution at temperature T (the value $T = 4\text{K}$ was used thoughout the paper).

SUPPLEMENT B. DIRAC THEORY FOR ARMCHAIR GNRS

For energies close to the Dirac points, electrons in graphene can be described effectively by a two-dimensional two-valley Dirac equation[18,19]. The boundary conditions of GNRs require the wave

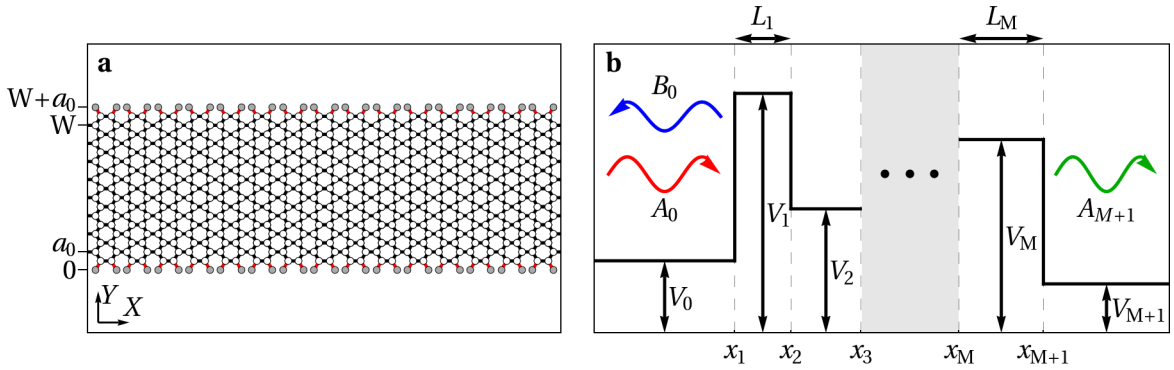

FIG. S4. **a**: Scheme of a GNR of width $W = 8a_0$. The boundary conditions for wave functions can be obtained by adding two rows of atoms (plotted in gray) at $y = 0,\ W + a_0$ and setting the wavefunction to 0 in those points. **b**: Transmission across a series of M potential steps. The incident plane wave with amplitude A_0 splits into a reflected and a transmitted component with amplitudes B_0 and A_{M+1}, respectively.

function to vanish on the (fictitious) sites just outside the GNR, *i.e.*, at $y = 0$ and $y = W + a_0$, where the y axis is perpendicular to the direction of the GNR and the lower edge of the GNR is located at $y = a_0/2$ (see Fig. S4 **a**). In the case of armchair GNRs, this affects both sublattices and the boundary conditions can be fulfilled by a superposition of two states from different valleys with the same energy $E = \hbar v_{\mathrm{F}}(k_\perp^2 + k_\parallel^2)^{1/2}$ and equal longitudinal momentum $\hbar\boldsymbol{k}_\parallel$, but with opposite transverse momentum $\pm\hbar\boldsymbol{k}_\perp$, measured from the Dirac points[20,28]. Here v_{F} is the Fermi velocity in graphene. Note that the effective description given by the Dirac equation holds as long as the $\mathbf{k}\cdot\mathbf{p}$ approximation remains valid, *i.e.*, for not too narrow GNRs.

Quantization of transverse momentum

Since the valley momenta $\boldsymbol{K}$ and $\boldsymbol{K}'$ can be chosen parallel to $\boldsymbol{k}_\perp$, the transverse wave function can be written $\phi_\perp(y) = \sin\big[(K + k_\perp)y\big]$ where $K = 4\pi/3a_0$. This function is evaluated on the honeycomb lattice with $y \in \mathbb{N}a_0/2$ and oscillates rapidly. The transverse momentum $\boldsymbol{k}_\perp$, however, is small and quantized by the conditions $\phi_\perp(W + a_0) = \phi_\perp(0) = 0$. The allowed values for $k_\perp$ are given by $(K + k_{\perp n})(W + a_0) = n\pi$, $n \in \mathbb{Z}$, and the spectrum reads

$$E_n(k_\parallel) = \pm\hbar v_{\mathrm{F}}\sqrt{k_{\perp n}^2 + k_\parallel^2}\,. \tag{S3}$$

Taking into account that W is an integer multiple of $a_0/2$, one finds that the spectrum is gapless if[28]

$$W = (3n_1 + 1)a_0/2\,, \quad n_1 \in \mathbb{N}\,. \tag{S4}$$

For asymmetric armchair GNR, as in Ref. 20, n_1 is even. For symmetric armchair GNR, W is an integer multiple of a_0 and n_1 is odd, such that $W = (3n-1)a_0$, $n \in \mathbb{N}$ implies a gapless spectrum.

In real samples there are small gaps even in the case (S4), which are due to edge effects[10,11] not included in the simple Dirac ansatz nor the homogeneous tight-binding formulation. In this work we consider symmetric armchair GNRs of width $W = \widetilde{n}a_0$, where the integer $\widetilde{n}$ is different from $3\mathbb{N}-1$, e.g., $W = 40a_0$. These have a gap anyway and are quite robust against edge effects. Then, the allowed values of the transverse momentum are

$$k_{\perp n} = \frac{\pi n}{3(W+a_0)} \ , \quad n = 1, 2, 4, 5, 7, 8, \ \ldots \ , \tag{S5}$$

and the half-gap is $E_0 = E_1(0) = \pi\hbar v_{\mathrm{F}}/[3(W+a_0)]$.

Transfer-matrix description of transmission

For geometries with potential depending only on the longitudinal coordinate x, the transverse momentum $\boldsymbol{k}_\perp$ together with the wave function $\phi_\perp(y)$ is conserved, and it suffices to solve for the longitudinal wave function $\phi_\parallel(x)$. We consider the transmission across a piecewise constant potential profile, as sketched in Fig. S4 **b**. The solution of the Dirac equation for each spin $\sigma = \pm 1$ and in each interval of constant potential value V is the superposition of two counter-propagating sublattice pseudo-spinors

$$\psi_\parallel(x) = A \begin{pmatrix} e^{-i\theta/2} \\ -e^{i\theta/2} \end{pmatrix} e^{ik_\parallel x} + B \begin{pmatrix} e^{+i\theta/2} \\ -e^{-i\theta/2} \end{pmatrix} e^{-ik_\parallel x} \ , \tag{S6}$$

with $\tan\theta = k_\parallel/k_\perp$ and $k_\parallel = [(E-V)^2/(\hbar v_{\mathrm{F}})^2 - k_\perp^2]^{1/2}$. The solution may be evanescent because Eq. (S6) holds also for $|E-V| < \hbar v_{\mathrm{F}}|k_\perp|$, when $k_\parallel$ and θ become imaginary. Then, the general form of the wave function in each slab j with potential V_j and momentum $k_\parallel = k_j$ is

$$\begin{pmatrix} e^{-i\theta_j/2} & e^{i\theta_j/2} \\ -e^{i\theta_j/2} & -e^{-i\theta_j/2} \end{pmatrix} \begin{pmatrix} A_j(x) \\ B_j(x) \end{pmatrix} =: S_j \begin{pmatrix} A_j(x) \\ B_j(x) \end{pmatrix} \ , \tag{S7}$$

where $A_j(x) = Ae^{ik_j x}$ and $B_j(x) = Be^{-ik_j x}$, such that

$$\begin{pmatrix} A_j(x_{j+1}) \\ B_j(x_{j+1}) \end{pmatrix} = \begin{pmatrix} e^{ik_j L_j} & 0 \\ 0 & e^{-ik_j L_j} \end{pmatrix} \begin{pmatrix} A_j(x_j) \\ B_j(x_j) \end{pmatrix} \equiv G_j \begin{pmatrix} A_j(x_j) \\ B_j(x_j) \end{pmatrix} , \tag{S8}$$

with $L_j = x_{j+1} - x_j$. At each junction, k_j changes but the wave function remains continuous

$$S_j \begin{pmatrix} A_j(x_j) \\ B_j(x_j) \end{pmatrix} = S_{j-1} \begin{pmatrix} A_{j-1}(x_j) \\ B_{j-1}(x_j) \end{pmatrix} . \tag{S9}$$

With the help of Eqs. (S8) and (S9), one writes down the transfer matrix for the whole system

$$\begin{pmatrix} A_{M+1} \\ B_{M+1} \end{pmatrix} = S_{M+1}^{-1} \widetilde{G}_M \dots \widetilde{G}_2 \widetilde{G}_1 S_0 \begin{pmatrix} A_0 \\ B_0 \end{pmatrix} , \tag{S10}$$

with $\widetilde{G}_j = S_j G_j S_j^{-1}$.

For the transmission problem depicted in Fig. S4 **b**, the boundary condition is no incoming electron from the right, $B_{M+1} = 0$. The reflection coefficient at the left is the ratio of reflected to incident current, $R = |B_0|^2/|A_0|^2$. For the transmission coefficient one has to take into account that the longitudinal momenta k_{M+1} and k_0 are different if $V_0 \neq V_{M+1}$, such that the ratio of transmitted to incident current is $T = (|A_{M+1}|^2 k_{M+1})/(|A_0|^2 k_0)$.

SUPPLEMENT C. BAND STRUCTURE OF THE UNBIASED LATTICE

The Dirac formalism allows us to analytically study the system in the limit $N \to \infty$, when the energy regions with high transmission become transmissions bands surrounded by energy regions with $T = 0$. For an unbiased lattice with identical barriers of width a and spacing b, there are only two different transfer matrices involved, $\widetilde{G}_a$ and $\widetilde{G}_b$. In the limit $N \to \infty$, the superlattice eigenfunctions have the Bloch phases $\exp(\pm iKl)$, that are the eigenvalues of the transfer matrix $\widetilde{G} = \widetilde{G}_a \widetilde{G}_b$ over one lattice period $l = a + b$. Thus, the dispersion relation $E(K, k_\perp)$ is obtained as $\cos(Kl) = \mathrm{Tr}(\widetilde{G})/2$, or again[22,24]

$$\cos(Kl) = \cos k_a l_a \cos k_b l_b + \frac{\cos\theta_a \cos\theta_b - 1}{\sin\theta_a \sin\theta_b} \sin k_a l_a \sin k_b l_b \ . \tag{S11}$$

If $|\,\mathrm{Tr}(\widetilde{G})/2| > 1$, there is no propagating solution with K real and E falls into the bandgap of the superlattice. In the main text, Fig. 2 **a** shows the bands of the infinite superlattice together with the transmission across a finite sample of five barriers.